

## TOPICAL REVIEW

## Kaon-Deuteron Scattering at Low Energies

A Sibirtsev<sup>†</sup> J Haidenbauer<sup>‡</sup> S Krewald<sup>‡</sup> and Ulf-G Meißner<sup>†‡</sup><sup>†</sup> Helmholtz-Institut für Strahlen- und Kernphysik (Theorie), Universität Bonn, Nußallee 14-16, D-53115 Bonn, Germany,<sup>‡</sup> Institut für Kernphysik, Forschungszentrum Jülich, D-52425 Jülich, Germany**Abstract.**

We review the experimental information on the  $K^+d$  reaction for  $K^+$ -meson momenta below 800 MeV/c. The data are analysed within the single scattering impulse approximation – utilizing the Jülich kaon-nucleon model – that allows to take into account effects due to the Fermi motion of the nucleons in the deuteron and the final three-body kinematics for the break-up and charge exchange reaction. We discuss the consistency between the data available for the  $K^+d \rightarrow K^+np$ ,  $K^+d \rightarrow K^0pp$  and  $K^+d \rightarrow K^+d$  reactions and the calculations based on the spectator model formalism.

PACS numbers: 11.80.-m; 13.75.Jz; 14.40.Aq; 24.10.-i; 25.70.Kk

**1. Introduction**

Recently the kaon-nucleon ( $K^+N$ ) interaction has attracted considerable interest because of the possible existence of the  $\Theta^+(1540)$  pentaquark. The  $K^+N$  system constitutes the only open hadronic decay channel for that resonance and, therefore, can be used to impose constraints on its width. The relevant isospin  $I=0$   $K^+N$  channel can be accessed experimentally only via kaon-deuteron ( $K^+d$ ) scattering and, therefore, pertinent analyses were performed through a direct inspection of data for the total  $K^+d$  cross section [1, 2] and the charge exchange reaction  $K^+d \rightarrow K^0pp$  [3, 4] in the relevant low-energy region. An examination [5] of data on the  $I=0$  total  $KN$  cross section was based on the isospin decomposition [6] of the  $K^+d$  total cross section. A reexamination of the  $KN$  partial wave (PW) analysis performed by Arndt et al. [7] in the light of the  $\Theta^+(1540)$  followed the same procedure as their earlier extraction of the  $I=0$   $K^+N$  amplitudes from the  $K^+d$  data.

In the present paper we provide an overview of the experimental information on the  $K^+d$  reaction. We concentrate on  $K^+$ -meson momenta below 800 MeV/c, say, because here the elementary  $KN$  reaction is predominantly elastic. Judging from the available data the contribution of inelastic channels ( $KN \rightarrow KN\pi$  etc.) to the cross sections is still only about 10 % at the upper end of this momentum range. Our main goal is to investigate whether the available  $K^+d$  data are consistent with each other and whether they can be consistently described using a  $KN$  model that reproduces the results of

up-to-date partial wave analyses. In particular, we utilize here the Jülich  $KN$  model I from Ref. [8]. The calculation of the  $K^+d$  observables is carried out in the single scattering impulse approximation. It allows to take into account effects due to the Fermi motion of the nucleons within the deuteron and the final three-body kinematics for the break-up reaction. The same formalism was applied by us previously in the analysis of the reaction  $K^+d \rightarrow K^0pp$ . In the present study we concentrate on the other  $K^+d$  channels where data are available, i.e. the reactions  $K^+d \rightarrow K^+np$  and  $K^+d \rightarrow K^+d$ . Note that this formalism forms also the basis of practically all  $KN$  partial wave analyses [9, 10, 11, 12, 13].

In the literature one can find only a small number of  $K^+d$  studies which were performed within a three-body (Faddeev) framework [14, 15, 16] or where at least corrections from multiple scattering were taken into account [17, 18, 19, 12, 20]. Furthermore, all those works concentrated on specific reactions and thus only on a rather limited set of the available  $K^+d$  data. With regard to  $K^+d$  coherent scattering the earliest Faddeev-type calculations [14], performed for kaon momenta of 110-230 MeV/c, suggested that in this momentum range multiple scattering corrections are of the order of 10-20%. This was later on confirmed by relativistic Faddeev calculations presented by Garcilazo [16] which covered the momentum range up to 1.5 GeV/c. His results also demonstrate that the total and the elastic  $K^+d$  cross section obtained from the full Faddeev calculation and from the impulse approximation practically coincide for kaon momenta of 400 MeV/c onwards, say.

Low-energy charge-exchange  $K^+d$  scattering was studied by Sañudo [20] within a multiple scattering expansion. He concluded that double-scattering terms due to the  $KN$  system and higher ones due to  $KN$  and  $NN$  systems had no observable effect on the charge-exchange  $K^+d$  cross section above 252 MeV/c. But even the effect of the  $NN$  final-state interaction turned out to be rather small [20].

In view of those results we anticipate that the impulse approximation that we use in our calculation should work rather well, in particular for momenta above 400 MeV/c where the bulk of the  $K^+d$  data are. Still effects from multiple scattering are expected to play a role for specific reaction kinematics. But the main question is, of course, whether those are manifest in the presently available empirical information on  $K^+d$  scattering, specifically, given the large error bars of the data. In any case, possible discrepancies between our calculation and experimental observables could be a signal for such effects.

In the present work we aim primarily for a direct comparison of our calculation with measured  $K^+d$  observables. But we consider also published  $K^+n$  data, which have been inferred from the reaction  $K^+d \rightarrow K^+np$ . The extraction of those  $K^+n$  scattering data from the deuteron reaction is based on the so-called spectator model, i.e. the single scattering impulse approximation. Thereby, it is assumed that the proton of the deuteron is the spectator and its only role in the  $K^+n$  interaction is due to the Fermi motion of the bound neutron. This is, in principle, a reliable method [21, 22, 23, 24, 25] as long as one measures the momentum distribution of the proton and one takes only those events which fulfil the so-called spectator condition, i.e. with the momentum

of the proton being less than the momentum of the neutron ( $p_p < p_n$ ). However, in practice often the spectator proton and the final neutron were not even identified in the corresponding  $K^+d$  experiments.

Another difficulty arises in case of the  $I=0$  total  $K^+N$  cross section. It was extracted [6, 26, 27, 28, 29, 30] from the total  $K^+d$  cross section utilizing the Glauber formalism, which originally was proposed for high energies [31, 32]. The shadowing corrections, which appear in these analyses, are based on substantial contributions from higher partial waves in the elementary scattering amplitude, i.e. it is assumed implicitly that the scattering amplitude dominates at forward direction. That is clearly not the case for  $KN$  scattering at low momenta.

Our paper is organized as follows. The Jülich model for the  $KN$  interaction is described in Sect. 2. In Sect. 3 we briefly give the formalism used for the  $K^+d$  charge exchange and break-up reactions and then we analyse the  $K^+d \rightarrow K^+np$  and  $K^+d \rightarrow K^0pp$  data. The formalism for coherent  $K^+$  scattering is given in Sect. 4 together with an analysis of the  $K^+d \rightarrow K^+d$  data. The total  $K^+d$  cross section is discussed in Sect. 5. The paper ends with summary.

## 2. The Jülich meson-exchange kaon-nucleon model.

The Jülich model of the  $KN$  interaction has been described in detail in Refs. [8, 33, 34, 35]. Thus, we summarize here only the main features. The Jülich meson-exchange model of the  $KN$  interaction was constructed along the lines of the Bonn  $NN$  model [36] and its extension to the hyperon-nucleon ( $YN$ ) system [37]. Specifically, this means that one has used the same scheme (time-ordered perturbation theory), the same type of processes, and vertex parameters (coupling constants, cutoff masses of the vertex form factors) fixed already by the study of those other reactions.

The diagrams considered for the  $KN$  interaction are shown in Fig. 1. Based on these diagrams the  $KN$  potential  $V$  is derived, and the corresponding reaction amplitude  $T$  is then obtained by a solving a Lippmann-Schwinger type equation defined by time-ordered perturbation theory:

$$T = V + VG_0T . \quad (1)$$

From this amplitude phase shifts and observables can be obtained in the usual way.

As evident from Fig. 1, the Jülich model contains not only single-meson and baryon exchanges, but also higher-order box diagrams with  $NK^*$ ,  $\Delta K$  and  $\Delta K^*$  intermediate states. Most vertex parameters involving the nucleon and the  $\Delta(1232)$  isobar were taken over from the Bonn  $NN$  potential. The coupling constants at vertices involving strange baryons are fixed from the  $YN$  model [37]. For the vertices involving mesons only, most coupling constants have been fixed by SU(3) relating them to the empirical  $\rho \rightarrow 2\pi$  decay. Exceptions are the  $KK\sigma$  and  $KK\omega$  coupling constants. The  $\sigma$  meson, with a mass of about 600 MeV, is not considered as a genuine particle but as a simple parametrization of correlated  $2\pi$ -exchange processes in the scalar-isoscalar channel. Therefore, its coupling

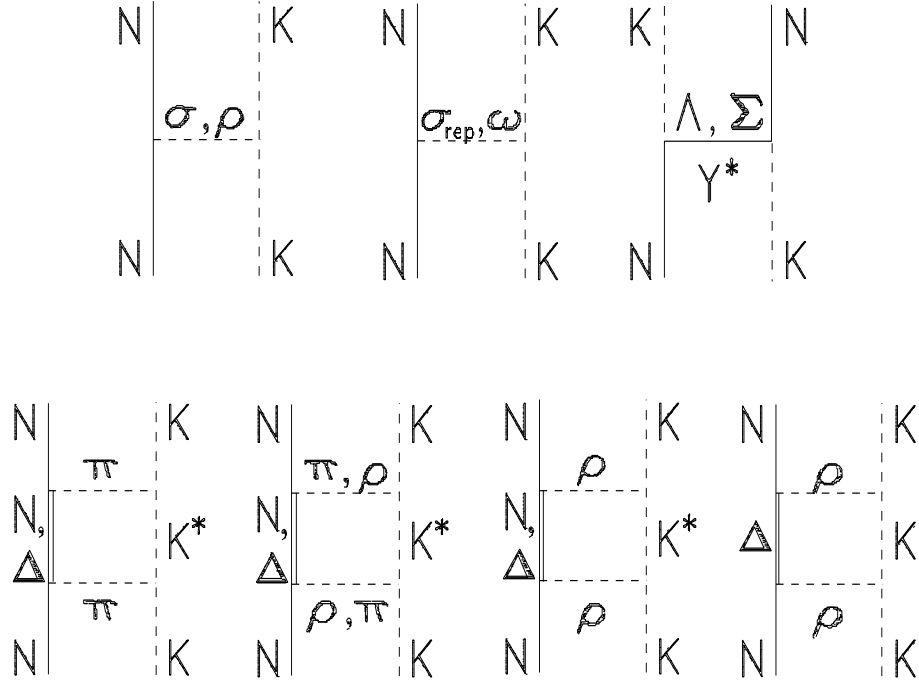


**Figure 1.** Meson-exchange contributions to  $KN$  scattering included in the Jülich model I [8].

strength cannot be taken from symmetry relations. In the initial Jülich model [33, 34, 35] it was simply adjusted by a fit to the  $KN$  data. In a subsequent investigation [8] the  $\sigma(600)$  and also the elementary  $\rho$  were replaced by a microscopic model for correlated  $2\pi$  and  $K\bar{K}$  exchange between kaon and nucleon, in the corresponding scalar-isoscalar and vector-isovector channels [8]. Starting point for this was a model for the reaction  $N\bar{N} \rightarrow K\bar{K}$  with intermediate  $2\pi$  and  $K\bar{K}$  states, based on a transition in terms of baryon, i.e.  $N$ ,  $\Delta$ ,  $\Lambda$  and  $\Sigma$ , exchange and a realistic coupled channel  $\pi\pi \rightarrow \pi\pi$ ,  $\pi\pi \rightarrow K\bar{K}$  and  $K\bar{K} \rightarrow K\bar{K}$  amplitudes. The contribution in the  $s$ -channel is then obtained by performing a dispersion relation over the unitarity cut.

Concerning the  $\omega$ -exchange it was found that a much larger strength than obtained from  $SU(3)$  would be required in order to get sufficient short-range repulsion for a reasonable description of the  $s$ -wave  $KN$  phase shifts [33]. Thus, a phenomenological, very short-ranged contribution was introduced in the potential (called  $\sigma_{rep}$ ) which then allowed to achieve a satisfactory description of the  $KN$  data [8]. Recently, it was shown that this phenomenological piece can be substituted by contributions from genuine quark-gluon exchange processes [38].

Since the results in Refs. [8, 38] indicate that the various  $KN$  models presented by the Jülich group yield a rather similar quantitative description of the  $KN$  data we will employ here only one of those model. Specifically, we will use the  $KN$  model I presented in Ref. [8]. Its parameters and the predictions for the  $KN$  phase shifts can be found in that reference, together with a comprehensive comparison with empirical

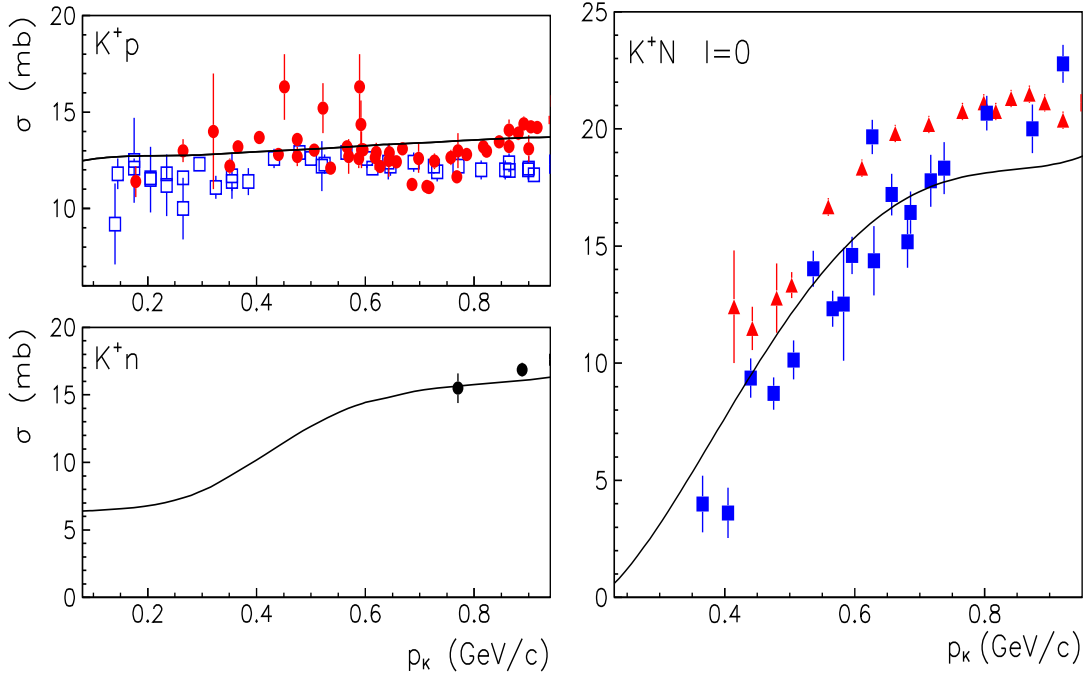


**Figure 2.** The  $K^+p$ ,  $K^+n$  and  $I=0$  cross sections as a function of the kaon momentum. The circles are data for the total ( $K^+p$ ,  $K^+n$ ) cross section, while open squares are the elastic cross section, all taken from Ref. [39]. The  $I=0$  results are taken from Refs. [6] (triangles) and [26, 27] (squares). The solid lines are the results of the Jülich  $KN$  model I [8].

$KN$  scattering data, and therefore we do not reproduce them here. However, we want to illustrate some specific features of the elementary  $K^+N$  results which are relevant for the present investigation on the  $K^+d$  reaction. Fig. 2 shows the  $K^+p$  and  $K^+n$  total and elastic cross sections as a function of the kaon momentum. The circles (squares) show the total (elastic) cross sections [39]. The solid lines are the results of the Jülich model for the total cross sections. The total and elastic cross sections for  $K^+p$  scattering are practically identical below kaon momenta of  $p_K \simeq 800$  MeV/c, i.e. inelasticities which can occur from  $p_K \simeq 520$  MeV/c onwards (due to the opening of the  $KN\pi$  channel) are negligible, and there is practically no energy dependence. The reaction channel corresponds to a pure  $I=1$  state. It is dominated by the  $s$ -wave amplitudes. Indeed, the available differential data for the  $K^+p$  reaction indicate isotropic angular spectra for  $p_K < 800$  MeV/c, cf. Ref. [8].

The elementary  $K^+n$  data can only be obtained indirectly from a study of the  $K^+d$  reaction. The Particle Data Group [39] lists only two data points for the total reaction cross section at low momenta. The Jülich model indicates a pronounced momentum dependence of the total  $K^+n$  cross section. It is primarily due to the  $p$ -wave contribution to the  $I=0$  amplitude, in particular the  $P_{01}$  partial wave, which is substantial already for low kaon momenta [8]. Note that the  $K^+n$  amplitude is given by (half of) the sum of the  $I=0$  and  $I=1$  isospin amplitudes. The total  $I=0$  cross section is shown in the right panel of Fig. 2 as a function of  $p_K$ . The Jülich model yields a reasonable reproduction

of the data collected in Refs. [6, 26, 27]. However, we want to emphasize that the  $I=0$   $KN$  cross section was extracted from the  $K^+d$  data at  $p_K < 800$  MeV/c by applying the high energy Glauber formalism [31, 32], which apparently introduces some ambiguities in the data evaluation. This point will be discussed in Sect.5.

### 3. Charge exchange and break-up reactions

#### 3.1. The formalism

A detailed and general description of the formalism for two-body scattering of a spin-zero and a spin-1/2 particle is given by Höhler [40]. Thus, we provide here only a brief overview. The  $KN$  reaction can be completely characterized by the spin-nonflip and spin-flip amplitudes  $f$  and  $g$  which, in terms of their partial wave projections, are given by

$$\begin{aligned} f_I &= \sum_{l=0}^{\infty} [(l+1)T_I^{l+} + lT_I^{l-}] P_l(\cos \theta), \\ g_I &= \sum_{l=1}^{\infty} \sin \theta [(T_I^{l+} - T_I^{l-}) P'_l(\cos \theta)]. \end{aligned} \quad (2)$$

Here  $l$  is the orbital angular momentum, and  $P_l$  and  $P'_l$  are Legendre polynomials and their derivatives, respectively. Furthermore,  $\theta$  is the scattering angle in the  $KN \rightarrow KN$  center of mass system and  $T_I^{l\pm}$  is the PW amplitude for the total angular momentum  $l \pm 1/2$  and isospin  $I$ , where the latter can be 0 or 1 for the  $KN$  system. The amplitudes of the three possible physical  $KN$  reactions are related to those in Eq. (2) by

$$K^+p \rightarrow K^+p : F_p = f_1 + f_C, \quad G_p = g_1, \quad (3)$$

$$K^+n \rightarrow K^+n : F_n = 1/2(f_1 + f_0), \quad G_n = 1/2(g_1 + g_0), \quad (4)$$

$$K^+n \rightarrow K^0p : F_{ex} = 1/2(f_1 - f_0), \quad G_{ex} = 1/2(g_1 - g_0), \quad (5)$$

where  $f_C$  stands for the Coulomb amplitude. The scattering amplitude for each of those reactions is then given in terms of the corresponding quantities  $F$  and  $G$  by

$$A = F + i\boldsymbol{\sigma} \cdot [\mathbf{k}_0 \times \mathbf{k}] G, \quad (6)$$

where  $\mathbf{k}_0, \mathbf{k}$  defines the direction of initial and final kaon, respectively and  $\boldsymbol{\sigma}$  is the Pauli matrix. The two-body scattering cross section and the polarization are given by

$$\frac{d\sigma}{d\Omega} = |A|^2 = |F|^2 + |G|^2, \quad P = \frac{2 \operatorname{Im}(FG^*)}{|F|^2 + |G|^2}. \quad (7)$$

It is clear that the amplitudes  $f_1$  and  $g_1$  can be obtained from an analysis of the  $K^+p \rightarrow K^+p$  elastic scattering data, while the determination of  $f_0$  and  $g_0$  relies on experiments with a deuteron target.

The differential cross section for the reaction  $K^+d \rightarrow K^+np$  is given in the impulse approximation by

$$\begin{aligned} \frac{d\sigma}{d\Omega} &= \int |A_d(k_0, k, q)|^2 \delta^4(k_0 + P - k - p - q) \frac{k^2 dk}{E_K} \frac{d^3 p}{E_p} \frac{d^3 q}{E_q}, \\ A_d &= A_n(k_0, k, q) \Psi(\mathbf{p}) + A_p(k_0, k, p) \Psi(\mathbf{q}), \end{aligned} \quad (8)$$

where  $k_0$ ,  $k$ ,  $P$ ,  $q$ , and  $p$  are the momenta of the initial and final kaon, of the deuteron and of the final neutron and proton, while  $E_K$ ,  $E_p$  and  $E_q$  are the total energies of the particles in the final state. Furthermore,  $\Psi$  is the deuteron wave function in momentum space:

$$\Psi(\mathbf{q}) = \psi_0(q) + \frac{1}{\sqrt{2}} \left( 3 \frac{(\mathbf{S} \cdot \mathbf{q})^2}{q^2} - 2 \right) \psi_2(q), \quad \mathbf{S} = \frac{1}{2}(\sigma_1 + \sigma_2). \quad (9)$$

The scattering amplitude is taken at  $t=(k-k_0)^2$  four-momentum transfer squared and at the squared invariant energy  $s=(k+q)^2$  or  $s=(k+p)^2$ , respectively. We should mention that in this expression not only effects from kaon rescattering and the  $(NN)$  final state interaction are neglected, in line with the impulse approximation, but also corrections due to the deuteron binding.

Note that, in principle, the  $K^+n$  and  $K^+p$  amplitudes enter off-shell in Eq. (8) because the interacting nucleon is off its mass shell. However, in an integration over the three-body phase space the dominant contribution to the cross section comes from the kinematics near zero spectator-momentum, where  $A_n$  and  $A_p$ , respectively, are close to their on-shell values and, therefore, in general one uses only the on-shell amplitudes.

In the application of the impulse approximation to the reaction  $K^+d \rightarrow K^+np$  and  $K^+d \rightarrow K^0pp$  one usually makes additional simplifications. First one neglects the  $d$ -wave component of the deuteron wave function. Secondly, one assumes that the energy dependence of the scattering amplitude is smooth within the range of integration of Eq. (8). Finally, one assumes that the elementary two-body  $KN$  amplitude enters into the three-body reaction in a kinematics where the scattered nucleon (and accordingly also the spectator) has zero momentum in the laboratory system. The latter two assumption allow to factorize  $|A_d|^2$  out of the integral of Eq. (8). Implementing these assumptions Stenger et al. [41] derived the following relations for the reactions  $K^+d \rightarrow K^0pp$  and  $K^+d \rightarrow K^+np$

$$\frac{d\sigma}{d\Omega}(K^+d \rightarrow K^0pp) = \left( |F_{ex}|^2 + \frac{2}{3}|G_{ex}|^2 \right) I_{ppt}(\theta) + \frac{1}{3}|G_{ex}|^2 I_{pps}, \quad (10)$$

$$\begin{aligned} \frac{d\sigma}{d\Omega}(K^+d \rightarrow K^+np) = & \left( |F_p|^2 + |F_n|^2 + \frac{2}{3}|G_p|^2 + \frac{2}{3}|G_n|^2 \right) I_{npt} \\ & + \frac{1}{3} \left( |G_p|^2 + |G_n|^2 \right) I_{nps} + 2\text{Re} \left( F_n^* F_p + \frac{2}{3} G_n^* G_p \right) J_{npt} \\ & - \frac{2}{3} \text{Re} \left( G_n^* G_p \right) J_{nps}, \end{aligned} \quad (11)$$

where  $I$  and  $J$  are the so-called deuteron inelastic form factors. Their subscripts specify whether the final  $pp$  or  $np$  pair is in a singlet ( $s$ ) or triplet ( $t$ ) state, respectively. In the plane wave approximation the six ( $I$  and  $J$ ) form factors reduce to

$$I_{pps} = I_0 + J_0, \quad I_{ppt} = I_0 - J_0, \quad I_{nps} = I_0, \quad I_{npt} = I_0, \quad J_{nps} = J_0, \quad J_{npt} = J_0, \quad (12)$$

where

$$I_0 = D \int \frac{u^2(p) + u^2(q)}{2} \delta^4(k_0 + P - k - p - q) \frac{k^2 dk}{E_K} \frac{d^3 p}{E_p} \frac{d^3 q}{E_q}, \quad (13)$$

$$J_0 = D \int u(p)u(q) \delta^4(k_0 + P - k - p - q) \frac{k^2 dk}{E_K} \frac{d^3 p}{E_p} \frac{d^3 q}{E_q} . \quad (14)$$

Here the kinematical factor  $D$  accounts for the transformation of the kaon scattering angle from laboratory  $K^+d$  system to the center of mass frame of the  $K^+N$  two-body system. The scattering amplitudes  $F$  and  $G$  are evaluated for the stationary spectator nucleon, i.e.

$$D = \frac{E_K}{k^2} \left. \frac{d(E_K + E_q)}{dk} \right|_{p=0} . \quad (15)$$

Let us emphasize here that Eq. (12) is valid only in the impulse approximation, which corresponds to a plane wave approximation for the wave function of the two final nucleons. For interacting nucleons the  $NN$  wave function is different for the singlet and triplet states. Moreover, the  $NN$  interaction in the final state might effect the forward scattering angles, specifically because this singlet interaction is rather strong [41].

In our calculations we use the  $KN$  amplitude of the Jülich model I [8] and the deuteron wave function from the recent charge-dependent Bonn  $NN$  potential [42]. We integrate the two-body amplitude over the full three-body phase space, i.e. we do not factorize the reaction amplitude. The calculations are performed in the deuteron rest frame. That allows us to compare our results directly to the majority of the experimental data which are naturally given in the laboratory system. In the few other cases we compare our results in the  $K^+N$  center-of-mass frame by performing a transformation into the two-body system under the assumption that the spectator nucleon is at rest, i.e. following Eq. (15). Since the published data are given in different frames we compile the relevant kinematical relations in an Appendix for the convenience of the reader.

### 3.2. The reaction $K^+d \rightarrow K^+np$

There are several experiments for the reaction  $K^+d \rightarrow K^+np$  and data are available for kaon momenta from 342 MeV/c onwards. The basic difficulty in comparing these experiments with our  $KN$  model comes from the reaction kinematics, which is not explicitly described in most of the papers. In general the available data are differential reaction cross sections as a function of the  $K$ -meson scattering angle, which are given either in the laboratory (deuteron rest) system or in the quasi two-body  $KN$  center-of-mass frame. The momentum of the spectator and/or of the scattered nucleon are often not specified or not measured explicitly. Thus, the reaction can involve kaon scattering on both the proton and neutron and therefore we add the corresponding amplitudes according to Eq. (8). This amplitude is then integrated over the full three-body phase space and without any cuts on the momenta of the final particles. This might be inadequate since the momenta and angles of the final proton and neutron can be limited due to the detector acceptance. However, without corresponding information such kinematical constraints cannot be implemented in the three-body integration.

Results of our calculations are presented in Fig. 3, together with data from Refs. [41, 43, 44]. The differential cross sections are shown as a function of the



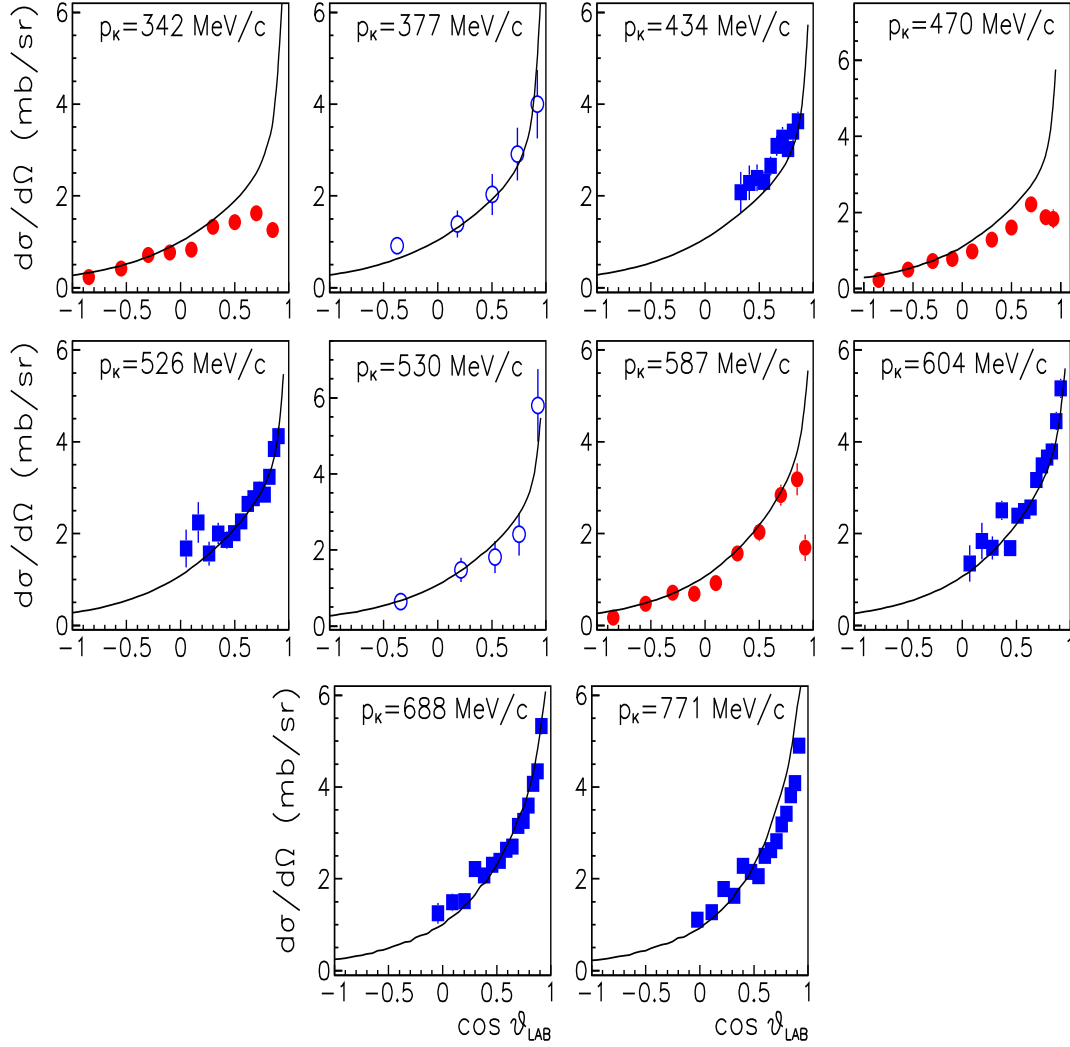


**Figure 3.** The  $K^+d \rightarrow K^+np$  differential cross section for different incident kaon momenta as a function of the kaon scattering angle in the laboratory system. The data are from Refs. [41] (open circles), [43] (filled circles), and [44] (squares). The solid lines show the result of our model calculation.

kaon scattering angle in the laboratory system. We use this frame in order to avoid ambiguities in the transformation from the deuteron rest frame, where the experiment was done, to the effective  $KN$  center-of-mass system. Note that this ambiguity is discussed in different experimental papers in detail and there are various prescriptions for that transformation, for instance the one given by Eq. (15).

The result at the lowest energy is due to Glasser et al. [43]. In this experiment the differential  $K^+d \rightarrow K^+np$  cross section was measured by identification of the 2-prong events. To distinguish between the  $K^+d \rightarrow K^0pp$  reaction, which also has two charged particles in the final state, an additional criteria on not-associated  $V$  tracks from the  $K^0 \rightarrow \pi^+\pi^-$  decay was imposed. Some misidentification of the reactions  $K^+d \rightarrow K^+np$  and  $K^+d \rightarrow K^+d$  comes from the proton and final deuteron tracks saturation and

difficulties to distinguish between them. While our calculation yields a good overall description of the data – at 342 MeV/c as well as at 587 MeV/c – there is obviously a discrepancy at forward angles to which we will come back below.

The reaction  $K^+d \rightarrow K^+np$  was also measured by Stenger et al. [41]. However, in their experiment it was not possible to separate the contributions from elastic  $K^+d \rightarrow K^+d$  scattering and from  $K^+d \rightarrow K^+np$  break-up. Therefore, the data shown by squares in Fig. 3 are the sum of the coherent and  $K^+d \rightarrow K^+np$  cross sections. The solid lines in Fig. 3 are model predictions for the genuine reaction  $K^+d \rightarrow K^+np$ . Obviously those results are already in pretty good agreement with the data reported in Ref. [41]. Thus, there is not much room left at forward angles for possible contributions from  $K^+d \rightarrow K^+d$  scattering. But, as we will show later, the coherent cross section is indeed very small and it strongly depends on the scattering angle due to the deuteron form factor.

Another  $K^+d \rightarrow K^+np$  experiment was performed by Damerell et al. [44]. The reaction was identified by detecting the  $K^+$ -meson using a time-of-flight (TOF) spectrometer. The squares in Fig. 3 show data that represent also the sum of the  $K^+d \rightarrow K^+d$  and  $K^+d \rightarrow K^+np$  differential cross sections. Again in this case our calculation for the  $K^+d \rightarrow K^+np$  reaction alone is in good agreement with the experimental results.

Let us come back to the data by Glasser et al. where the experiment shows a forward suppression, contrary to the theory. In this context let us recall that while comparing our  $K^+d \rightarrow K^0pp$  calculations [4] with the charge exchange data we did not detect any discrepancy at forward angles. On the other hand, from Eq. (10) one can see that the singlet  $pp$  form factor  $I_{pps}$  enters only via the spin-flip term  $G_{ex}$ , which itself is small and vanishes at forward angles. The spin non-flip part of the amplitude,  $F_{ex}$ , is multiplied by the form factor  $I_0 - J_0$  of Eq. (12) that originates from the spin triplet  $pp$  interaction which also vanishes at forward direction. The  $K^+d \rightarrow K^0pp$  charge exchange differential cross section is thus suppressed at forward angles, which is clearly seen in our results in Ref. [4] that are also discussed in the next subsection. Therefore, it would be difficult to see any inadequacy of the employed elementary  $KN$  amplitudes or of the impulse approximation at small angles because the corresponding model results are automatically reduced.

For the  $K^+d \rightarrow K^+np$  reaction the situation is somewhat different. Since the spin non-flip amplitude  $F$  dominates the reaction and both ( $I_0$  and  $J_0$ ) form factors do not vanish at forward angles, there is no suppression of the differential cross section at forward angles in the model calculation. Therefore, the discrepancy with the Glasser data [43] in forward direction, cf. Fig. 3, could indeed be a signal for a failure of the impulse approximation, say. On the other hand, and may be more likely, it could be simply due to ambiguities in the data evaluation, specifically, because we do get nice agreement with the forward data within the same energy range provided by other groups [41, 44]. In this context we would like to mention that the authors of Ref. [43] did not include their  $K^+d \rightarrow K^+np$  data in their own  $KN$  partial wave analysis nor did they

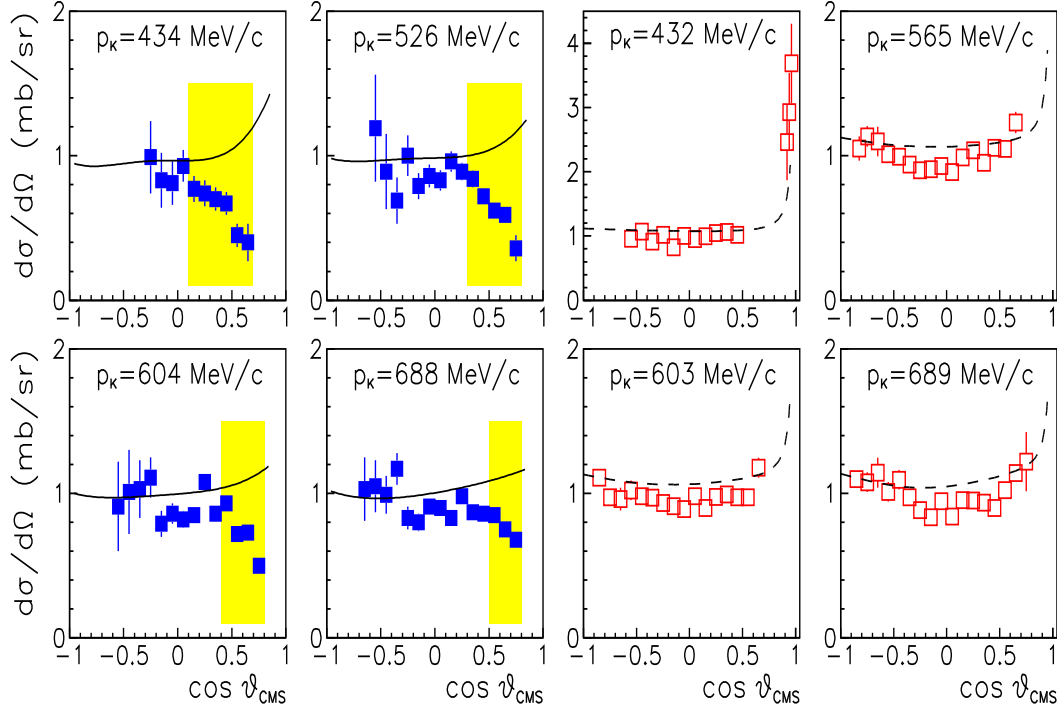


**Figure 4.** The  $K^+p \rightarrow K^+p$  differential cross section for different incident kaon momenta as a function of the kaon scattering angle in the center of mass system. The filled squares show the results extracted from the  $K^+d \rightarrow K^+pn$  reaction [44] with reconstructed neutron spectator. The shaded areas indicate the angular range where data analysis was considered to be ambiguous by the authors. The open squares are the differential cross sections measured on a hydrogen target [45]. The solid lines show our calculation for the reaction  $K^+d \rightarrow K^+pn$  (assuming that the  $n$  is the spectator), while the dashed lines indicate our (elementary)  $K^+p \rightarrow K^+p$  results.

confront the results of that analysis with the measured  $K^+d \rightarrow K^+np$  differential cross sections.

Besides data on the reaction  $K^+d \rightarrow K^+np$  one can also find experimental results for the elementary  $K^+n \rightarrow K^+n$  process in the literature [44, 46]. In order to obtain such data one has to invoke the spectator model and one has to isolate those  $K^+d \rightarrow K^+np$  events with either a proton or a neutron as spectator, i.e. where either the proton or the neutron momentum fulfils the spectator condition  $p_p < p_n$  or  $p_n < p_p$ , respectively. However, in case of the data of Damerell et al. [44] it remains to some extent unclear how the experimental separation between the reactions with a spectator proton or neutron was done since, as already said earlier, the direction and momentum of only one of the outgoing particles was measured and it was not possible to specify exactly the kinematics of each event. Nonetheless their analysis had the ambitious goal to extract also  $K^+p$  cross sections from  $K^+d \rightarrow K^+pn$  events with a spectator neutron and compare them with the free differential cross section for  $K^+p$  scattering. Such a comparison constitutes a crucial test for extracting (elementary)  $KN$  cross sections from measurements on a deuteron target, provided that it is performed with a sensible data set.

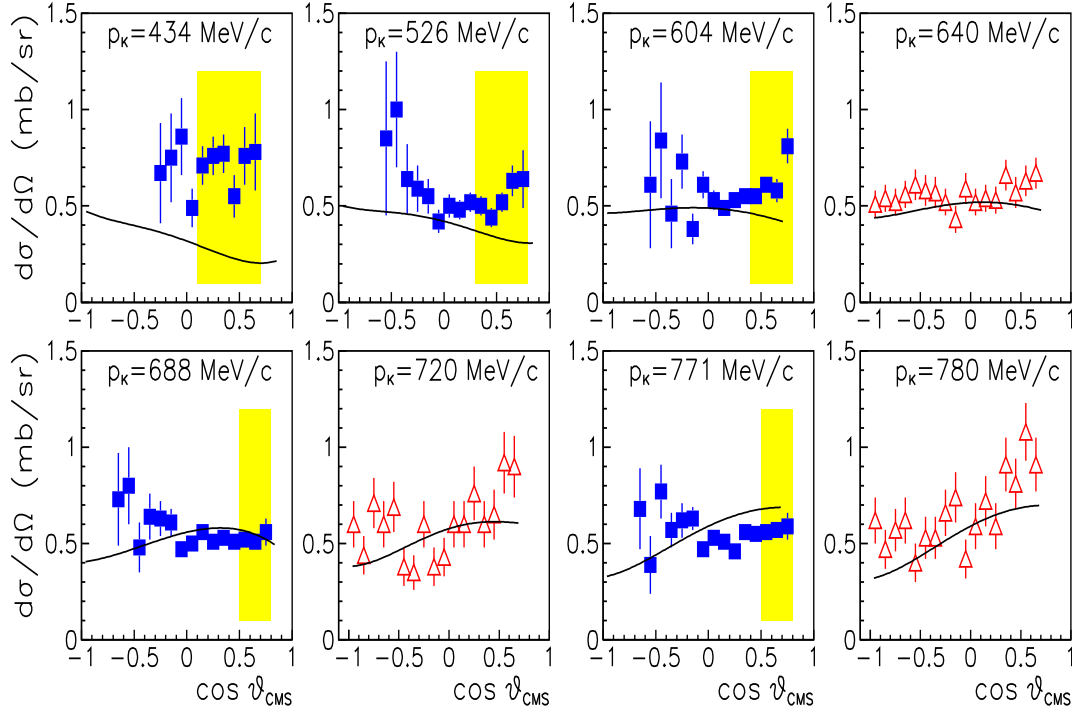


**Figure 5.** The  $K^+n \rightarrow K^+n$  differential cross section for different incident kaon momenta as a function of the kaon scattering angle in the center of mass system. The experimental results were extracted from the  $K^+d \rightarrow K^+np$  reaction with reconstructed neutron spectator; squares show the data from Ref. [44], while the triangles were taken from Ref. [46]. The shaded areas indicate the angular range where the data analysis was considered to be ambiguous by the authors. The solid lines show our calculations for the  $K^+d \rightarrow K^+np$  reaction (assuming that the  $p$  is the spectator).

The  $K^+p \rightarrow K^+p$  differential cross sections extracted by Damerell et al. from their  $K^+d \rightarrow K^+np$  data are shown by the filled squares in Fig. 4. The shaded areas indicate the region where, according to the authors [44], possible uncertainties in the treatment of the final proton and effects due to coherent scattering affect the data analysis. The solid lines in Fig. 4 show our calculations for the  $K^+d \rightarrow K^+np$  reaction with a spectator neutron, i.e. with the amplitude  $A_p$  of Eq. (6). The calculations and data are shown in the  $K^+N$  c.m. frame in order to enable a comparison with data as well as calculations for the free  $K^+p$  reaction, which are presented at the right side of Fig. 4. Those data (open squares in Fig. 4) are  $K^+p \rightarrow K^+p$  differential cross sections measured [45] with a hydrogen target and at kaon momenta close to that studied in the  $K^+d \rightarrow K^+np$  experiment [44]. The corresponding model predictions are given by the dashed line. Obviously both sets of data are in rough agreement outside of the shaded areas. But there is indeed a strong disagreement at forward angles.

Fig. 5 contains the  $K^+n \rightarrow K^+n$  differential cross section extracted from the  $K^+d \rightarrow K^+np$  for different kaon momenta and as a function of the  $K^+$ -meson scattering angle in the  $KN$  c.m. system. The squares are the results from Ref. [44], while triangles show the measurements from Ref. [46]. Note that in the latter experiment the spectator

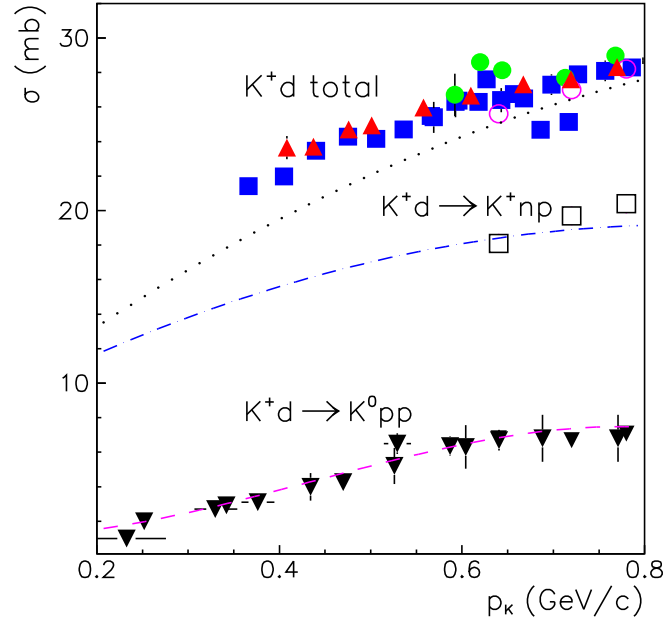


**Figure 6.** The total  $K^+d$  cross section and the integrated  $K^+d \rightarrow K^+np$  and  $K^+d \rightarrow K^0pp$  reaction cross sections as a function of the kaon momentum. The dashed and dash-dotted lines are the results of our model calculations for the  $K^+d \rightarrow K^0pp$  and  $K^+d \rightarrow K^+np$  cross sections, respectively, while the dotted line is their sum. Data for the  $K^+d$  total cross section are from Refs. [26, 27] (filled squares), [6] (filled triangles), [28] (filled circles) and [30] (open circles). The  $K^+d \rightarrow K^+np$  data are from [30] (open squares), while the  $K^+d \rightarrow K^0pp$  cross section are from [44, 48] (inverse triangles).

condition for the proton was imposed in selecting the events. Specifically, only those events were accepted where the momentum of the spectator proton was between 100 and 250 MeV/c [46]. The data disagree at forward angles by roughly a factor of two. Our model calculation for the  $K^+d \rightarrow K^+np$  reaction with spectator proton (solid lines Fig. 5) is in reasonable agreement with the differential cross sections measured by Giacomelli et al. [46]. There is also a rough agreement with the data by Damerell et al. if one disregards the shaded area, except for the lowest kaon momentum  $p_K = 434$  MeV/c.

Because most of the  $K^+d \rightarrow K^+np$  differential cross sections were measured only for limited scattering angles and/or there were ambiguities in the data analysis and, specifically, in the separation of the break-up and coherent reactions, these data were never used to obtain integrated cross sections. Nonetheless, we present here predictions of our model for the integrated  $K^+d \rightarrow K^+np$  reaction cross section. Corresponding results are shown in Fig. 6 (dashed-dotted line) as function of kaon momentum. We also indicate (by the open squares) the only published concrete data for the  $K^+d \rightarrow K^+np$  integrated cross section [30] that we found in the literature. These three points are reasonably described by the model calculation.

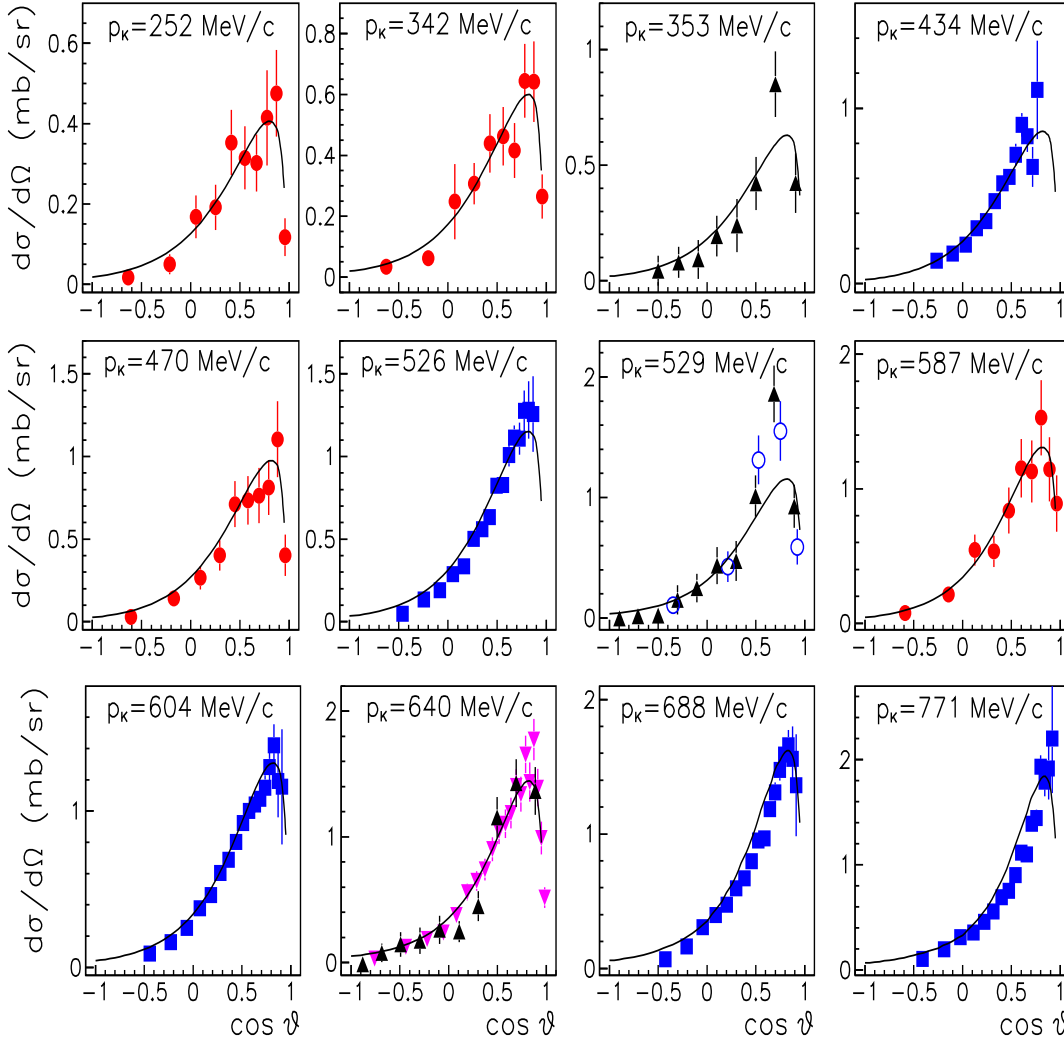


**Figure 7.** The  $K^+d \rightarrow K^0pp$  differential cross section for different incident kaon momenta as a function of the kaon scattering angle in the laboratory system. The data are taken from Refs. [41] (open circles) [43] (filled circles), [44] (squares), [47] (inverse triangles), and [48] (triangles). The solid lines show our model calculations.

### 3.3. The reaction $K^+d \rightarrow K^0pp$

The  $K^+d \rightarrow K^0pp$  reaction can be uniquely reconstructed by detecting two charged particles in the final state in addition to the associated V track from the  $K^0 \rightarrow \pi^+\pi^-$  decay. As a consequence the experimental error bars are smaller than those for the other break-up channels. An additional advantage of the charge exchange reaction is due to the isospin structure, cf. Eq. (5). The  $K^+d \rightarrow K^0pp$  amplitude is proportional to the difference between the  $I=1$  and  $I=0$  amplitudes. On the other hand, since the  $K^+d \rightarrow K^+pn$  reaction was measured without identification of the spectator proton the break-up amplitude amounts to the sum of 3/2 of the  $I=1$  and only 1/2 of the  $I=0$  amplitudes. Therefore the charge exchange  $K^+d$  reaction is much more sensitive to the  $I=0$  amplitude and, in turn, much more decisive for the determination of the  $I=0$

amplitude in a partial wave analysis.

A detailed comparison of our model calculation with the available experimental information for the  $K^+d \rightarrow K^0pp$  charge exchange reaction at kaon momenta below 640 MeV/c was already presented in Ref. [4]. For completeness we show those results again and we include predictions for two more momenta, namely 688 and 771 MeV/c, cf. Fig. 7. Obviously, there is almost perfect agreement between the data and the calculations, which might be not surprising since the Jülich model describes rather well the  $I=0$  phase shifts, which were extracted from the charge exchange reaction. It is worthwhile to note that the  $K^+d \rightarrow K^0pp$  cross section at  $p_K=252$  MeV/c constitutes the lowest energy at which data for  $K^+d$  are available, and it can be well reproduced by the model calculation within the impulse approximation.

Fig. 6 shows the integrated  $K^+d \rightarrow K^0pp$  cross section as a function of the kaon momentum. Also here there is nice agreement of our calculation with the data, taken from Refs. [44, 48].

## 4. Coherent $K^+d$ scattering

### 4.1. Formalism

The formalism for the coherent  $K^+d \rightarrow K^+d$  scattering is given in detail in Refs. [19, 41, 49, 50, 51]. Here we only list the formulas relevant for our calculation. Within the single scattering impulse approximation the elastic scattering amplitude is given by

$$A_d = \int d^3p \Psi(\mathbf{p}) [A_p(k_0, k, p) + A_n(k_0, k, p)] \Psi(\mathbf{p}-\mathbf{q}/2), \quad (16)$$

with  $\mathbf{q}=\mathbf{k}_0-\mathbf{k}$  being the three-momentum transferred from the initial to the final kaon. Assuming again that the  $KN$  scattering amplitude is a smooth function of  $\mathbf{p}$  as compared with the momentum dependence of the deuteron wave function the amplitude can be taken out of the integral in Eq. (16), and the  $KN$  amplitude can be taken approximately at  $\mathbf{p}=0$  [19, 51, 52]. Apparently, such an approximation is even more justified for coherent scattering than for the break-up reactions. If one neglects also the deuteron  $d$ -wave component then the coherent differential cross section is given by

$$\frac{d\sigma}{d\Omega} = [|F_p + F_n|^2 + \frac{2}{3}|G_p + G_n|^2] \Phi_S^2(\frac{q}{2}), \quad (17)$$

where  $\Phi_S$  is the spherical form factor of the deuteron evaluated from the  $s$ -wave deuteron wave function alone [19, 41].

In some of the analyses [43] the  $d$ -wave part of the deuteron wave function was taken into account in order to estimate the single scattering contribution at large  $q$  or large scattering angles. In that case the coherent differential cross section is given by

$$\frac{d\sigma}{d\Omega} = |F_p + F_n|^2 \left[ \Phi_S^2(\frac{q}{2}) + \Phi_Q^2(\frac{q}{2}) \right] + \frac{2}{3}|G_p + G_n|^2 \Phi_M^2(\frac{q}{2}), \quad (18)$$

where  $\Phi_S$ ,  $\Phi_Q$  and  $\Phi_M$  are the spherical, quadrupole and magnetic form factors of the deuteron, i.e.

$$\Phi_S = \Phi_a + \Phi_b,$$

$$\begin{aligned}
\Phi_Q &= 2\Phi_c - \frac{\Phi_d}{\sqrt{2}} \\
\Phi_M &= \Phi_a - \frac{\Phi_b}{2} + \frac{\Phi_c}{\sqrt{2}} + \frac{\Phi_d}{2},
\end{aligned}
\tag{19}$$

with

$$\begin{aligned}
\Phi_a(q) &= \int dr \, j_0(qr) |u(r)|^2, \\
\Phi_b(q) &= \int dr \, j_0(qr) |w(r)|^2, \\
\Phi_c(q) &= \int dr \, j_2(qr) u(r) w(r), \\
\Phi_d(q) &= \int dr \, j_2(qr) |w(r)|^2,
\end{aligned}
\tag{20}$$

where  $j_0$  and  $j_2$  are the zeroth and second order spherical Bessel functions, respectively. In general one should take into account all these form factors in analysing scattering at large angles and for evaluating the contribution from multiple scattering. That is why we provide the single scattering formalism here explicitly. As before we utilize the deuteron wave functions of the CD Bonn potential [42].

#### 4.2. Results

The  $K^+d$  coherent scattering at kaon momenta below 800 MeV/c was measured in several experiments [43, 50, 53]. It is clear from Eqs. (16) and (18) that the angular distribution for coherent scattering is dominated by the deuteron form factor and the  $I=1$  component of the  $K^+N$  scattering amplitude. That actually leads to the conclusion [43] that the  $K^+d \rightarrow K^+d$  reaction should not be too sensitive to the  $I=0$  amplitude, or in other words, one has to expect large uncertainties when one tries to extract the  $I=0$  amplitude from  $K^+d$  coherent scattering.

In Fig. 8 we compare our model results with the available data on the differential  $K^+d \rightarrow K^+d$  cross section. The measurement of Glasser et al. [43] (filled circles) was performed at the kaon momenta of 342, 470, and 587 MeV/c. The solid lines show our calculations by Eq. (18), while the dashed lines are results from Eq. (16). While the data at forward angles are well reproduced we find a strong discrepancy at large angles. This is not too surprising because it is known from Faddeev calculations of the  $K^+d$  system that multiple-scattering effects play an important role at backward angles in elastic  $K^+d$  scattering [15, 16]. Specifically, the corresponding results presented in Ref. [16] demonstrate very clearly that the description of the data of Glasser et al. improves significantly in this angular region as compared to the impulse approximation. For the ease of comparison we included the curves of Ref. [16] in our Fig. 8 (dotted lines). At the same time those Faddeev calculations confirm that the impulse approximation works rather well in forward direction, i.e. for laboratory angles smaller than 60 degrees ( $\cos \theta > 0.5$ ), say. Incidentally, since this angular range provides the bulk contribution to the integrated elastic  $K^+d$  cross section one expects that the impulse approximation



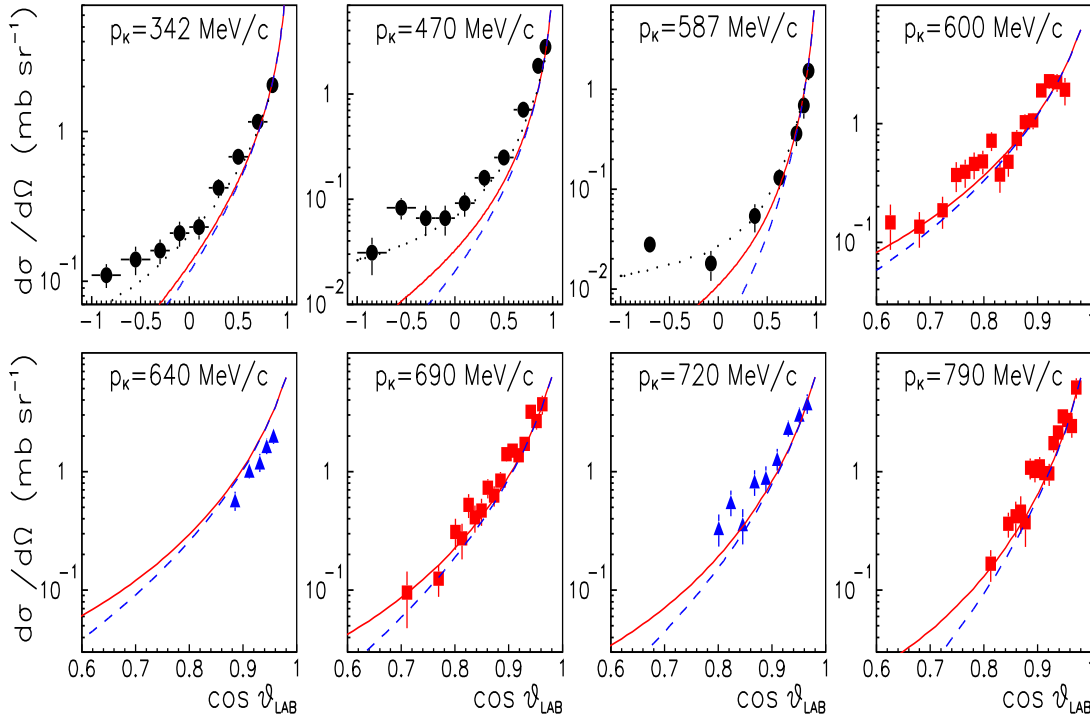


**Figure 8.** The  $K^+d \rightarrow K^+d$  differential cross section for different kaon momenta as a function of the kaon scattering angle in the laboratory system. The data are taken from Ref. [43] (circles), [50] (triangles), and [53] (squares). The solid lines show our calculations by Eq. (18), while the dashed lines are results obtained with Eq. (16). The dotted lines show the relativistic Faddeev calculations [16].

should yield also reliable results for the latter observable. This is indeed the case, judging from the results presented in Fig. 1 of Ref. [16], where one sees practically no difference to the Faddeev calculation even for rather small energies.

As a side remark we would like to point out that none of the calculations can reproduce an apparent structure visible in the tail of the coherent angular spectrum at kaon momentum of 470 MeV/c. But it is possible that this structure is simply a statistical fluctuation in the data.

Let us mention in this context that the authors of Ref. [43] were able to reproduce the angular spectra both at small and large angles within the impulse approximation by suitably adjusting the  $I = 0$   $KN$  PW amplitudes to the  $K^+d \rightarrow K^+d$  reaction, which resulted in large  $p$ -wave contributions. However, in that case the obtained PW amplitudes are in strong conflict with the solution from their own analysis of the  $K^+d \rightarrow K^0pp$  reaction [43].

The squares in Fig. 8 show the data of Sakitt et al. [53]. Their measurement covers only forward angles and it is well described by our calculations. The same is the case for the results by Giacomelli et al. [50], which are shown by triangles in the Fig. 8.

Results for the integrated  $K^+d$  cross sections are presented in Fig. 9 as a function of the kaon momentum. In the left panel we show results for the elastic  $K^+d \rightarrow K^+d$

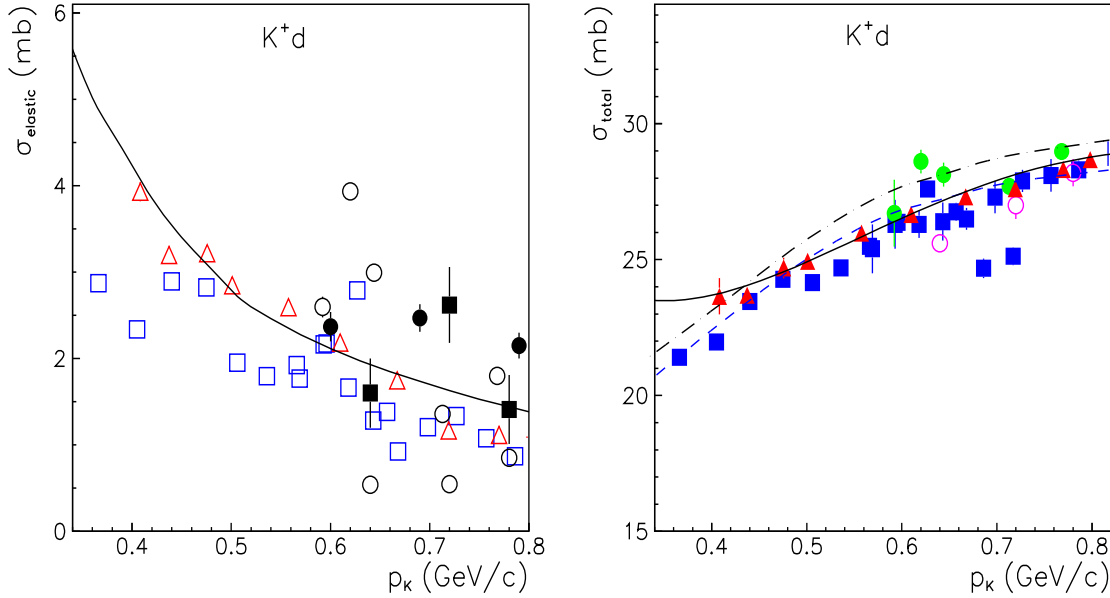


**Figure 9.** The  $K^+d$  elastic (left) and total (right) cross section as a function of the kaon momentum. The data for the  $K^+d$  total cross section are taken from Refs. [6, 26, 27, 28, 30]. Available data on the integrated  $K^+d$  elastic cross section from direct measurements are given by filled symbols [50, 53]. The open symbols represent values obtained by subtracting our model results for the integrated  $K^+d \rightarrow K^+np$  plus  $K^+d \rightarrow K^0pp$  cross sections from the various data on the  $K^+d$  total cross section. The solid lines represent our model calculation, where the total cross section is simply the sum of all partial cross sections. The dash-dotted line is the result of Eq. (21) with  $\delta\sigma=0$ , while the dashed line is obtained with a cross section defect evaluated via Eq. (23) with the ratios  $\rho_p$  and  $\rho_n$  taken from the Jülich  $KN$  model.

scattering cross section. Here the closed symbols are data from direct measurements while the open symbols represent values obtained by subtracting our model results for the integrated  $K^+d \rightarrow K^+np$  plus  $K^+d \rightarrow K^0pp$  cross sections from the various data on the  $K^+d$  total cross section. These (deduced) elastic cross sections fluctuate substantially. It is simply a reflection of the discrepancy between these data for the total  $K^+d$  cross sections, specifically in case of Bowen et al. [26, 27] and Carroll et al. [6]. The solid line is our prediction for the elastic cross section which is roughly in line with the directly measured and the deduced data. As already mentioned above, we expect that the impulse approximation leads to reliable results over the whole considered momentum range.

## 5. The total $K^+d$ cross section

The total  $K^+d$  cross section is presented in the right panel of Fig. 9. The data are the same as in the Fig. 6. The solid line represents the sum of the calculated  $K^+d \rightarrow K^+np$ ,  $K^+d \rightarrow K^0pp$  and the elastic  $K^+d$  cross sections. Our result is in good agreement with the data for kaon momenta  $p_K \geq 0.45$  GeV/c. This is not too surprising since our

model calculation yields reasonable descriptions of the differential cross sections in all contributing individual reaction channels.

In the extraction of the  $I=0$  isospin cross section (cf. Fig. 2) from  $K^+d$  experiments [6, 26, 27, 29] the total  $K^+d$  cross section is written as [31, 32]

$$\sigma_{K^+d}^{tot} = \sigma_{K^+p}^{tot} + \sigma_{K^+n}^{tot} - \delta\sigma, \quad (21)$$

where  $\sigma_{K^+p}^{tot}$  and  $\sigma_{K^+n}^{tot}$  are the total  $K^+p$  and  $K^+n$  cross sections (cf. Fig. 2) and  $\delta\sigma$  is the so-called cross section defect. The first two terms on the right hand side of Eq. (21) follow from the application of the optical theorem to the  $K^+d$  amplitude within the impulse approximation. Specifically, when taking the  $K^+N$  scattering amplitude out of the  $p$  integral in Eq. (16), one ends up with an integration over the deuteron wave function. This yields the deuteron form factor which is one at  $\mathbf{q}=0$  by definition, and thus  $A_d(0)=A_p(0)+A_n(0)$ . Applying then the optical theorem to  $A_d$ ,

$$\sigma_{tot} = \frac{4\pi}{p_K} \text{Im } A_d(0), \quad (22)$$

one obtains the first two terms. The third term,  $\delta\sigma$ , is usually derived from the double scattering amplitude according to the Glauber theory [31, 32], which should be valid for high energies. At low energies the term should contain additional corrections due to multiple scattering.

To inspect how large this correction is one can assume  $\delta\sigma=0$  and compare the outcome of Eq. (21) with the data. The corresponding result is shown by the dash-dotted line in Fig. 9. We see that the cross section defect amounts to about 1 mb or to about 4% of the total  $K^+d$  cross section.

In all experiments [6, 26, 27, 28, 29, 30] devoted to the extraction of the total  $I=0$  isospin  $K^+N$  cross section from the measured total  $K^+d$  cross section Eq. (21) was used with  $\delta\sigma$  explicitly given by

$$\delta\sigma = \frac{\langle r^{-2} \rangle}{4\pi} [2\sigma_{K^+p}\sigma_{K^+n}(1-\rho_p\rho_n) - \frac{1}{2}\sigma_{K^+p}(1-\rho_p)^2 - \frac{1}{2}\sigma_{K^+n}(1-\rho_n)^2], \quad (23)$$

where  $\rho_p$  and  $\rho_n$  are the ratios of the real to imaginary part of the kaon scattering amplitude on proton and neutron, respectively, while  $\langle r^{-2} \rangle = 0.3 \text{ fm}^{-2}$  is the parameter of the Glauber model introduced during the evaluation of the double scattering amplitude and corresponds to the averaged distance between proton and neutron in the deuteron. The correction according to Eq. (23) includes charge exchange [54] in the double scattering. At high energies the scattering amplitude are almost imaginary and  $\rho_p = \rho_n = 0$ . Therefore,  $\delta\sigma$  is given in terms of the  $K^+p$  and  $K^+n$  cross section. Since  $\sigma_{K^+p}^{tot}$  is experimentally known one can easily extract  $\sigma_{K^+n}^{tot}$  from  $\sigma_{K^+d}^{tot}$ .

For very low momenta the imaginary part of the  $KN$  forward scattering amplitude approaches zero, while the real part does not. Furthermore, the real part of the scattering amplitude in forward direction,  $\text{Re } A(0)$ , for  $K^+p$  scattering is known experimentally. Corresponding results [55] are shown in Fig. 10 together with the ratio  $\rho_p$ . Note that there is no experimental information on  $\text{Re } A(0)$  for  $K^+n$  scattering. The solid lines in Fig. 10 show the predictions of the Jülich  $KN$  model, while the dashed lines

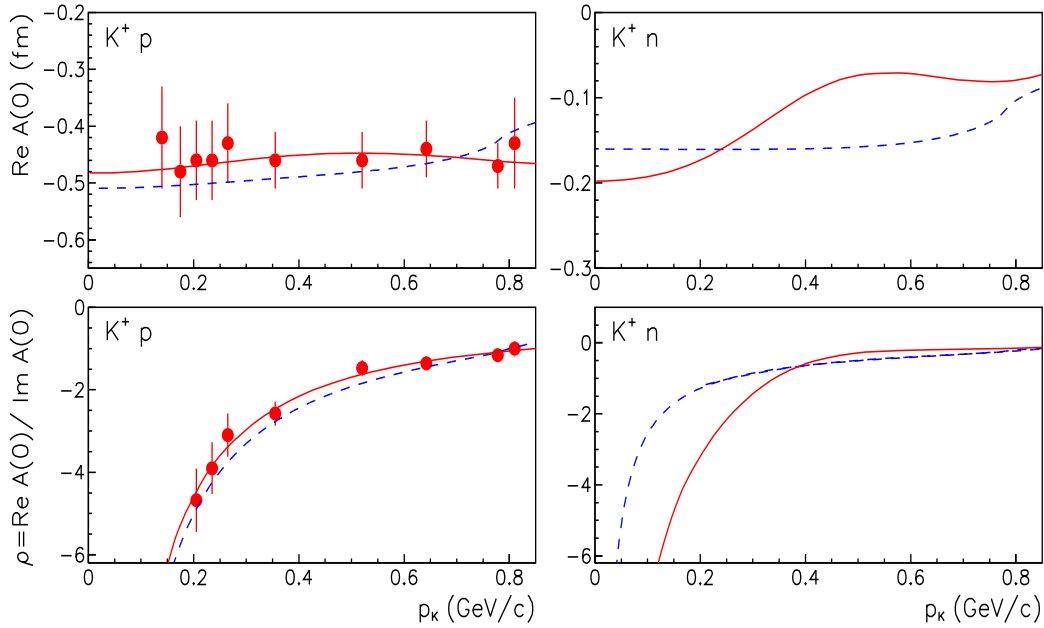


**Figure 10.** The real parts of the  $K^+p$  and  $K^+n$  forward scattering amplitudes in the laboratory system and the ratios  $\rho$  of the real to imaginary parts as a function of the kaon momentum. The data were taken from Ref. [55]. The solid lines are the predictions of the Jülich model I, while the dashed lines show the results from dispersion relations [56].

show results of a calculation by dispersion relations [56]. For  $K^+p$  scattering both results are similar and also in agreement with the data. However, not unexpectedly, there is a substantial disagreement between the dispersion calculation and the Jülich result for the forward  $K^+n$  scattering amplitude, in particular for small momenta. Presumably the variations of the  $I=0$  cross section in Fig. 2 between different experiments are due to different parameters used in the application of Eq. (23).

The result for the total  $K^+d$  cross section based on Eq. (21) with  $\delta\sigma$  evaluated via Eq. (23) for the  $KN$  amplitude of the Jülich model is presented by the dashed line in Fig. 9. It is in remarkable qualitative agreement with the data over the whole considered momentum range.

## 6. Summary

We investigated the  $K^+d$  reaction at kaon momenta below 800 MeV/c. The available data on the channels  $K^+d \rightarrow K^0pp$ ,  $K^+d \rightarrow K^+pn$  and  $K^+d \rightarrow K^+d$  and the total  $K^+d$  reaction cross section were compared with a calculation based on the Jülich  $KN$  model. The angular spectra were computed within the single scattering impulse approximation taking into account Fermi motion of the nucleons in the deuteron and the final three-body kinematics for the charge exchange and break-up reactions. A compact summary of the considered data and the achieved results is given in Table 1.

It was found that the experimental results for the reaction  $K^+d \rightarrow K^0pp$  published

in Refs. [41, 43, 44, 47, 48] can be very well reproduced down to the kaon momentum of 252 MeV/c, i.e. even for the smallest momentum where data are available. There seems to be practically no space for additional effects with regard to possible corrections to the impulse approximation, although one would expect that such corrections might become more and more relevant when approaching the threshold. It is worthwhile to notice the agreement between the data and the calculations, despite the fact that in the experiments the momentum of the spectator proton was not detected and no additional cuts were imposed. While the shape of the momentum spectrum of the spectator proton allows to examine the applicability of the single scattering impulse approximation [52], a momentum cut permits for the isolation of the multiple scattering contribution. These conditions were neither monitored nor imposed in the experiments.

The reaction  $K^+d \rightarrow K^0pp$  constrains to a large extent the  $I=0$   $KN$  scattering amplitude because of two reasons. First, it can be uniquely identified by the two charged particles in the final state associated with a  $V$  track from the  $K^0 \rightarrow \pi^+\pi^-$  decay and therefore the data are relatively precise. Second, the charge exchange amplitude is the half difference between the  $I=1$  and  $I=0$  amplitudes, i.e. it contains a sizeable isoscalar contribution. Note that the  $I=1$  amplitude can be uniquely determined from the  $K^+p \rightarrow K^+p$  data.

The data on the reaction  $K^+d \rightarrow K^+pn$  turned out to be practically unimportant for the  $KN$  phase-shift analyses although there is a large amount of experimental results for this reaction. This has to do with the fact that, in general the spectator nucleon from the  $K^+d \rightarrow K^+pn$  reaction was not measured and therefore the amplitude for the break-up reaction is the sum of the  $K^+p \rightarrow K^+p$  and  $K^+n \rightarrow K^+n$  amplitudes. In that case the  $K^+d \rightarrow K^+pn$  amplitude is dominated by the  $I=1$  component, i.e. its contribution constitutes 3/4 of the total reaction amplitude while only 1/4 come from the  $I=0$  component. Moreover, there are also difficulties in the final particle identification, especially in the  $K^+$ -meson forward direction, where the various experimental groups have tried to resolve that problem in different ways. As a consequence in this angular range the results from different measurements are partly in contradiction with each others. It turned out that our model calculation is in nice agreement with the  $K^+d \rightarrow K^+pn$  data from Refs. [41, 44], but it fails to reproduce the results from Ref. [43] at forward angles.

We also analysed those experiments [44, 46] which aimed to identify the spectator nucleon and to measure the elementary scattering using the (other) nucleon in the deuteron. Although we reasonably reproduce the  $K^+n \rightarrow K^+n$  results from Ref. [46], our calculations are partly in strong disagreement with data from Ref. [44]. We should say that in the latter experiment the spectator nucleon was not measured but indirectly reconstructed applying a somewhat obscure event selection procedure and, in addition, the authors admit that there are extremely large uncertainties of the data for forward angles. In view of that it might be not too surprising that there are discrepancies.

One of the goals of the study in Ref. [44] was to compare the  $K^+p \rightarrow K^+p$  results obtained with a deuteron target with those obtained on a free proton [45] and to verify

the spectator model formalism. The obtained experimental results on a bound proton are partly in strong disagreement with those from free protons, depending on the angular range. However, we attribute this discrepancy to the just mentioned uncertainties in the experimental spectator identification method and not to the validity of the spectator formalism.

Finally we analysed  $K^+d \rightarrow K^+d$  elastic scattering. Here our calculations within the impulse approximation reproduce the data [43, 50, 53] quite well at forward angles but exhibit substantial deviations at backward angles and at kaon momenta below 600 MeV/c, say. Although this discrepancy accounts for not more than 10% of the total elastic  $K^+d \rightarrow K^+d$  cross section it explicitly indicates that strong few-body effects play a role in this specific kinematical regime. Indeed, relativistic  $K^+d$  Faddeev calculations performed by Garcilazo [16] can reproduce the  $K^+d \rightarrow K^+d$  scattering fairly well also at large angles.

Combining our results for the  $K^+d \rightarrow K^0pp$ ,  $K^+d \rightarrow K^+pn$  and  $K^+d \rightarrow K^+d$  reaction channels we computed the total  $K^+d$  reaction cross section which turned out to be in good agreement with the measurements given in Refs. [6, 26, 27, 28, 30].

In conclusion, the bulk of the available  $K^+d$  data base for  $K^+$ -meson momenta below 800 MeV/c, which comprises differential and integrated cross sections for the reaction channels  $K^+d \rightarrow K^0pp$ ,  $K^+d \rightarrow K^+pn$ , and  $K^+d \rightarrow K^+d$ , can be described quantitatively and consistently within the single scattering impulse approximation utilizing a  $KN$  model that reproduces the results of up-to-date partial-wave analyses. This means that the data are indeed consistent with each other (save a few exceptions discussed above) where one has to emphasize that many observables were measured by three or more independent groups at various beam momenta. The success of the single scattering impulse approximation also implies that for the kinematics where the data are available multiple scattering effects are presumably negligible. In fact, the only clear evidence for the presence of such effects were found in the  $K^+d$  elastic cross section at backward angles. Finally, the nice reproduction of the  $K^+d$  data based on a standard  $KN$  model leaves also little room for contributions of a  $\Theta^+(1540)$  pentaquark. There is no obvious signal in the data that such a resonance is needed. On the other hand, a  $\Theta^+(1540)$  with a rather small width of 1 MeV or less can always be accommodated, as we have already shown in Ref. [4]. This conclusion is in agreement with results of the most recent searches for the  $\Theta^+(1540)$  in the reaction  $\gamma p \rightarrow \bar{K}^0 K^+ n$  and  $\gamma p \rightarrow \bar{K}^0 K^0 p$  [57, 58].

## Acknowledgments

A.S. acknowledges useful discussions with D. Bugg. This work was partially supported by Deutsche Forschungsgemeinschaft through funds provided to the SFB/TR 16 “Subnuclear Structure of Matter”. This research is part of the EU Integrated Infrastructure Initiative Hadron Physics Project under contract number RII3-CT-2004-506078. A.S. acknowledges support by the COSY FFE grant No. 41760632 (COSY-085)

and the JLab grant SURA-06-C0452.

## Appendix A.

For convenience we collect here kinematical formulas used for the transformation of the experimental results on differential cross section from one system to another. Let  $A$  be a Lorentz invariant amplitude. The differential cross section for the two-body reaction  $a+b \rightarrow c+d$  in the laboratory frame is given as

$$\frac{d\sigma}{d\Omega_{lab}} = \frac{p_c^2}{64\pi^2 m_b p_a} \frac{|A|^2}{(E_a + m_b)p_c - p_a E_c \cos \theta_{lab}} , \quad (\text{A.1})$$

where  $p_a$ ,  $E_a$ ,  $p_c$ ,  $E_c$  are the momenta and energies of the particles  $a$  and  $c$  in the laboratory frame, while  $\theta_{lab}$  is scattering angle of particle  $c$  with respect to the beam direction in laboratory. Here  $m_a = m_c$  and  $m_b = m_d$  are the masses of the particles. The differential cross section in the center of mass is given as

$$\frac{d\sigma}{d\Omega_{cms}} = \frac{1}{64\pi^2 s} |A|^2 , \quad (\text{A.2})$$

where the invariant collision energy squared is

$$s = m_a^2 + m_b^2 + 2E_a m_b . \quad (\text{A.3})$$

The Lorentz invariant cross section is defined as

$$\frac{d\sigma}{dt} = \frac{|A|^2}{64\pi s q_a^2} , \quad (\text{A.4})$$

where

$$q_a^2 = \frac{(s - m_a^2 - m_b^2)^2 - 4m_a^2 m_b^2}{4s} ,$$

$$t = -2q_a^2(1 - \cos \theta_{cms}) = 2m_a^2 - 2E_a E_c + 2p_a p_c \cos \theta_{lab} . \quad (\text{A.5})$$

The relation between the scattering angles in center of mass and laboratory frames is given as

$$\tan \theta_{lab} = \frac{2m_b \sqrt{s} \sin \theta_{cms}}{(s - m_a^2 - m_b^2) \cos \theta_{cms} + s + m_a^2 - m_b^2} . \quad (\text{A.6})$$

Furthermore  $E_c$  depends on the scattering angle and in more compact form can be expressed in terms of invariants as

$$E_c = \frac{s + t - m_a^2 - m_b^2}{2m_b} , \quad (\text{A.7})$$

while  $t$  is related to  $\theta_{cms}$  and  $\theta_{lab}$  by Eq. (A.5).

## References

- [1] Gibbs W R 2004 *Phys. Rev. C* **70** 045208 [arXiv:nucl-th/0405024]
- [2] Nussinov S arXiv:hep-ph/0307357.
- [3] Cahn R N and Trilling G H 2004 *Phys. Rev. D* **69** 011501 [arXiv:hep-ph/0311245]

- [4] Sibirtsev A, Haidenbauer J, Krewald S and Meißner Ulf-G 2004 *Phys. Lett. B* **599** 230 [arXiv:hep-ph/0405099]
- [5] Haidenbauer J and Krein G. 2003 *Phys. Rev. C* **68** 052201 [arXiv:hep-ph/0309243]
- [6] Carroll A S *et al* 1973 *Phys. Lett. B* **45** 531
- [7] Arndt R A, Strakovsky I I and Workman R L 2003 *Phys. Rev. C* **68** 042201, Er 2002 *ibid. C* **69** 019901 [arXiv:nucl-th/0308012]
- [8] Hoffmann M, Durso J W, Holinde K, Pearce B C and Speth J 1995 *Nucl. Phys. A* **593** 341
- [9] Martin B R 1975 *Nucl. Phys. B* **94** 413
- [10] Watts S J, Bugg D V, Gibbs W R 1980 *Phys. Lett. B* **95** 323
- [11] Nakajima K *et al* 1982 *Phys. Lett. B* **112** 80
- [12] Hashimoto K 1984 *Phys. Rev. C* **29** 1377
- [13] Hyslop J S, Arndt R A, Roper L D, Workman R L 1992 *Phys. Rev. D* **46** 961; CNS DAC Services (<http://gwdac.phys.gwu.edu/>)
- [14] Hetherington J H and Schick L H 1965 *Phys. Rev.* **138** B1411
- [15] Sañudo J 1982 *Phys. Rev. C* **26** 2682; 1983 *Nucl. Phys. A* **402** 462
- [16] Garcilazo H 1988 *Phys. Rev. C* **37** 2022
- [17] Gourdin M and Martin A 1959 *Il Nuovo Cim.* **14** 722
- [18] Andrade S C B and Ferreira E 1981 *Nucl. Phys. A* **364** 253
- [19] Hashimoto K 1983 *Phys. Rev. C* **27** 1572
- [20] Sañudo J 1984 *Phys. Lett.* **145B** 11; 1985 *Phys. Lett.* **165B** 251
- [21] Meyer H O and Niskanen J 1993 *Phys. Rev. C* **47** 2474
- [22] Duncan F *et al* 1998 *Phys. Rev. Lett.* **80** 4390; Hahn H *et al* 1999 *Phys. Rev. Lett.* **82** 2258
- [23] Calén H *et al* 1998 *Phys. Rev. C* **58** 2667
- [24] Złomańczuk J 2001 *AIP Conference Proceedings* **503** 211
- [25] Moskal P arXiv:hep-ph/0408162.
- [26] Bowen T *et al* 1970 *Phys. Rev. D* **2** 2599
- [27] Bowen T *et al* 1973 *Phys. Rev. D* **7** 22
- [28] Bugg D V *et al* 1968 *Phys Rev* **168** 1466
- [29] Cool R L *et al* 1970 *Phys. Rev. D* **1** 1887
- [30] Giacomelli G *et al* 1972 *Nucl. Phys. B* **37** 577
- [31] Glauber R J 1955 *Phys. Rev.* **100** 242
- [32] Franco V and Glauber R J 1966 *Phys. Rev.* **142** 1195
- [33] Büttgen R, Holinde K, Müller–Groeling A, Speth J and Wyborny P 1990 *Nucl. Phys. A* **506** 586
- [34] Büttgen R, Holinde K, Lohse D, Müller–Groeling A, Speth J and Wyborny P 1990 *Z. Phys. C* **46** S167.
- [35] Wyborny P, Hoffmann M, Holinde K and Speth J 1993 *Phys. Rev. C* **48** 1376
- [36] Machleidt R, Holinde K and Elster Ch 1978 *Phys. Rep.* **149** 1
- [37] Holzenkamp B, Holinde K and Speth J 1989 *Nucl. Phys. A* **500** 485
- [38] Hadjimichef D, J. Haidenbauer J and Krein G 2002 *Phys. Rev. C* **66** 055214 [arXiv:nucl-th/0209026]
- [39] Eidelman S *et al* 2004 *Phys. Lett. B* **592** 1
- [40] Höhler 1983 *G Landolt-Börnstein New Series* **9** Springer
- [41] Stenger V J *et al* 1964 *Phys. Rev.* **134** B1111.
- [42] Machleidt R 2001 *Phys. Rev. C* **63** 024001 [arXiv:nucl-th/0006014]
- [43] Glasser R G *et al* 1977 *Phys. Rev. D* **15** 1200
- [44] Damerell C J S *et al* 1975 *Nucl. Phys. B* **94** 374
- [45] Adams C J *et al* 1973 *Nucl. Phys. B* **66** 36
- [46] Giacomelli G *et al* 1973 *Nucl. Phys. B* **56** 346
- [47] Giacomelli G *et al* 1972 *Nucl. Phys. B* **42** 437
- [48] Slater W *et al* 1961 *Phys. Rev. Lett.* **7** 378
- [49] Sidhu D P and Quigg C *Phys. Rev. D* **7** 755



- [50] Giacomelli G *et al* 1974 *Nucl. Phys. B* **68** 285
- [51] Bertocchi L and Capella A 1967 *Nuovo Cim.* **51** A369
- [52] Alberi G and Bertocchi L 1969 *Nuovo Cim.* **63** A285
- [53] Sakitt M, Skelly J and Thompson J A *Phys. Rev. D* **12** 3386
- [54] Wilkin C 1966 *Phys. Rev. Lett.* **17** 561
- [55] Dumbrais O V, Dumbrais T Y and Queen N M 1971 *Fort. Phys.* **19** 491
- [56] Sibirtsev A and Cassing W 1998 *Nucl. Phys. A* **641** 476
- [57] Battaglieri M *et al* 2006 *Phys. Rev. Lett.* **96** 042001
- [58] De Vita R *et al* 2006 arXiv:hep-ex/0606062

**Table 1.**  $K^+d$  data analyzed in the present study. Note that the results for the reaction  $K^+n \rightarrow K^+n$  are not directly from a measurement but were extracted from the reaction  $K^+d \rightarrow K^+np$  as described in the text. For the quality rating we use the following categories: excellent agreement of data and theory (\*\*\*), minor deviation (\*\*), major deviation (\*), where in the latter two cases we provide a concrete description of the deficiency in a footnote.

	Ref.	$p_K$ [MeV/c]	type	quality
$K^+d \rightarrow K^+np$				
Stenger	[41]	377, 530	$d\sigma/d\Omega$	***
Glasser	[43]	342 - 587	$d\sigma/d\Omega$	* †)
Damerell	[44]	434 - 771	$d\sigma/d\Omega$	***
Giacomelli	[30]	640 - 780	$\sigma_{total}$	***
$K^+d \rightarrow K^0pp$				
Stenger	[41]	530	$d\sigma/d\Omega$	** ††)
Glasser	[43]	252 - 587	$d\sigma/d\Omega$	***
Damerell	[44]	434 - 771	$d\sigma/d\Omega$	***
Giacomelli	[47]	640	$d\sigma/d\Omega$	***
Slater	[48]	353 - 640	$d\sigma/d\Omega$	** ††)
Damerell	[44]	434 - 771	$\sigma_{total}$	***
Slater	[48]	252 - 640	$\sigma_{total}$	***
$K^+d \rightarrow K^+d$				
Glasser	[43]	342 - 587	$d\sigma/d\Omega$	** ‡)
Giacomelli	[50]	640, 720	$d\sigma/d\Omega$	***
Sakitt	[53]	600 - 790	$d\sigma/d\Omega$	***
Giacomelli	[50]	640 - 780	$\sigma_{elastic}$	* ‡‡)
Sakitt	[53]	600 - 790	$\sigma_{elastic}$	* ‡‡)
Carroll	[6]	408 - 798	$\sigma_{total}$	** §)
Bowen	[26]	366 - 717	$\sigma_{total}$	** §)
Bowen	[27]	569 - 786	$\sigma_{total}$	** §)
Bugg	[28]	592 - 768	$\sigma_{total}$	** §)
Giacomelli	[30]	640 - 780	$\sigma_{total}$	** §)
$K^+n \rightarrow K^+n$				
Damerell	[44]	434 - 771	$d\sigma/d\Omega$	* §§)
Giacomelli	[46]	640 - 780	$d\sigma/d\Omega$	** §§§)

†): inconsistency with other data and model calculation at forward angles.

††): inconsistency with other data and model calculation for  $p_K \approx 530$  MeV/c and for  $\cos \theta \geq 0.5$ .

‡): shortcoming of model calculation at backward angles.

‡‡): inconsistency between the data.

§): some inconsistencies between the data.

§§): ambiguities in the data analysis at forward angles.

§§§): statistical fluctuations in the data.